A&A, 711, A218 (2026)
https://doi.org/10.1051/0004-6361/202659502

Astronomy & Astrophysics

Possible extragalactic positron annihilation signal

Thomas Siegert[1,⋆] and Hiroki Yoneda[2,3,4,5]

[1] Julius-Maximilians-Universität Würzburg, Fakultät für Physik und Astronomie, Institut für Theoretische Physik und Astrophysik, Lehrstuhl für Astronomie, Emil-Fischer-Str. 31, D-97074 Würzburg, Germany
[2] The Hakubi Center for Advanced Research, Kyoto University, Yoshida Ushinomiyacho, Sakyo-ku, Kyoto 606-8501, Japan
[3] Department of Physics, Kyoto University, Kitashirakawa Oiwake-cho, Sakyo-ku, Kyoto 606-8502, Japan
[4] RIKEN Nishina Center, 2-1 Hirosawa, Wako, Saitama 351-0198, Japan
[5] Kavli Institute for the Physics and Mathematics of the Universe (WPI), UTIAS, The University of Tokyo, 5-1-5 Kashiwanoha, Kashiwa, Chiba 277-8583, Japan

Received 18 February 2026 / Accepted 17 May 2026

ABSTRACT

Context. With 20 years of INTEGRAL/SPI observations, the most detailed map of the positron annihilation line at 511 keV was created. While the central bulge and extended disk are readily recognised in this map, several hotspots at high latitude regions may either be imaging artefacts or true signals.

Aims. We discuss possible extragalactic positron annihilation signals from hotspots in this map. We also calculate a cosmological positron annihilation signal as a contribution to the cosmic gamma-ray background (CGB).

Methods. For this investigation, we compared 511 keV emission hotspots away from the Galactic plane with a high velocity cloud column density map as well as with the catalogue of local volume galaxies (LVGs) up to 25 Mpc.

Results. In particular, the Magellanic Stream in the southern and Complex C in the northern sky match the brightest hotspots. This might indicate that the positron production rate inside the Milky Way is higher than measured from the Galactic interstellar medium alone, potentially up to 10^{44} s^{-1}. In addition, we can explain other hotspots by the cumulative effect of LVGs in the selected regions. The CGB contribution from positron annihilation might be sub-dominant on the percent level. However, depending on the true intrinsic annihilation spectrum, in particular, depending on the positron injection energy for in-flight annihilation and the star formation rate per galaxy, a much higher imprint beyond 10% is possible above several MeV.

Conclusions. If these findings are confirmed, next-generation MeV telescopes will, for the first time, identify individual extragalactic 511 keV sources. In particular, several dwarf spheroidal galaxies with fluxes of up to $(1–2) \times 10^{-5}$ ph cm^{-2} s^{-1}, the galaxies M31 and M33, and some of their satellites, with potentially several 10^{-6} ph cm^{-2} s^{-1} each, may be detected.

Key words. ISM: clouds – cosmic rays – cosmic background radiation – gamma rays: galaxies

1. Introduction

With more than 20 years of data from the Spectrometer onboard the International Gamma-Ray Astrophysics Laboratory (INTEGRAL/SPI; Winkler et al. 2003; Vedrenne et al. 2003), Yoneda et al. (2025, hereafter HY25) performed a Richardson-Lucy (RL) image reconstruction of the positron annihilation line at 511 keV. The strong Galactic bulge emission was seen together with an undoubted signal from the Galactic disk. In addition to these now well-established emission features, several also highly significant emission regions away from the Galactic bulge and plane emerged. While image reconstruction is often prone to artefacts, systematic tests applied to the dataset, including bootstrapping of the full dataset and background-only image reconstructions, confirmed the persistence of some emission regions. These high-latitude ($|b| \gtrsim 15°$) emission features, which may also have been seen with the Compton Spectrometer and Imager (COSI; Tomsick et al. 2024) balloon experiment in 2016 (Kierans et al. 2017; Siegert et al. 2020), demand a thorough discussion and interpretation.

Nearby extragalactic sources up to ∼15 Mpc (redshift $z \lesssim 0.0034$, corresponding to a line shift of $\lesssim$2 keV) might contribute in the imaged 511 keV bin from 508–514 keV as the emission line would not be shifted out of this band. Higher redshifts might also contribute, but the line would be shifted towards lower energies, and most of the emission would be found outside the studied bin. At distances larger than 15 Mpc, that is, about the distance to the Virgo cluster, the cosmological redshift would start moving larger fractions of the γ-ray line out of the selected window. For example, at the distance of the Fornax cluster at ≈19 Mpc ($z = 0.0046$), the line would already be centred at 508.7 keV, so 50% of the total line flux at most would be included from Fornax. At a distance to the Coma cluster (≈100 Mpc, $z = 0.0231$), the line would be entirely shifted out of the 508–514 keV bin as the centroid would be at 499.5 keV. There are more than 1500 galaxies in the local volume, the so-called local volume galaxies (LVGs; Karachentsev et al. 2004; Karachentsev 2005; Karachentsev et al. 2013), whose cumulative signal could be within reach of the SPI sensitivity. Some emission hotspots, even though not statistically significant in themselves, might be coincident with groups of LVGs in the supergalactic plane. However, the exposure of INTEGRAL is highly non-uniform in the sky, so that not every nearby galaxy group would contribute. High-exposure regions off the Galactic plane are found in the regions of Andromeda, Ursa Major, Hydra, Sextans, and Virgo. In addition to these regions, two more hotspots were found in which hardly any nearby galaxy is located. These regions appear to coincide with high-velocity

⋆ Corresponding author: thomas.siegert@uni-wuerzburg.de

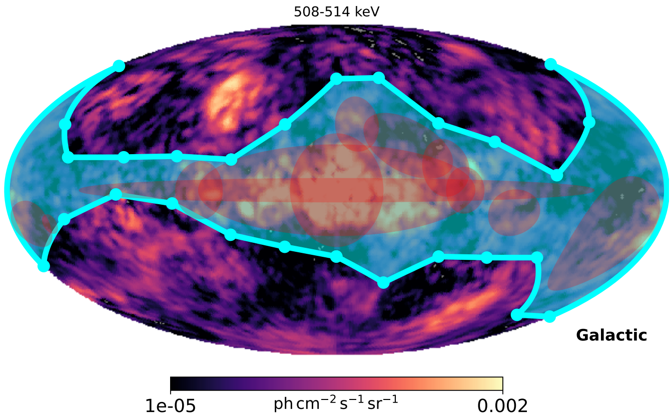

Fig. 1. RL 511 keV map from HY25 in a Mollweide projection with high contrast and reduced lower threshold. The masked region (cyan) was chosen to remove the Galactic bulge, thin and thick disk, nearby massive star regions such as Scorpius Centaurus ($\Delta\ell \approx [290°, 360°]$, $\Delta b \approx [-10°, +30°]$), Orion-Eridanus ($[180°, 230°]$, $[-50°, -5°]$), Taurus ($[160°, 180°]$, $[-25°, -5°]$), Perseus ($[155°, 165°]$, $[-25°, -15°]$), Vela ($[245°, 280°]$, $[-25°, +5°]$), Carina ($[285°, 295°]$, $[-5°, +5°]$), and Cygnus ($[70°, 90°]$, $[-10°, +10°]$), plus a margin of a few degrees to take the surrounding HI regions into account. The lower threshold defines the cut regions.

clouds (HVCs; Westmeier 2018), and in particular, the Magellanic Stream.

We assess the reconstructed 511 keV fluxes around HVCs, the Magellanic Stream, and large accumulations of nearby galaxies (Sect. 2), and we discuss whether their origin might be astrophysical (Sects. 3 and 4). Further, we calculate an expected cosmological positron annihilation signal (Sect. 5) by assuming different dependences on the star formation rate (SFR) and compare it to current measurements of the cosmic gamma-ray background (CGB). We summarise our findings in Sect. 6.

2. Artefact, Galactic or extragalactic?

In Fig. 1 we show the RL 511 keV map from HY25 in the band 508–514 keV from 20.5 yr of INTEGRAL/SPI data with high contrast and a reduced lowered flux threshold to emphasise the high-latitude excesses. The masked regions include the bulge, the disk, and some nearby emission regions that might be associated with the β^{+}-decay of ^{26}Al, such as Orion-Eridanus, Perseus, Taurus, Scorpius-Centaurus, Cygnus, Carina, and Vela, as well as large parts of the Galactic anti-centre, including the Crab. In Fig. 2 we then show the same map overlaid with nearby gas clouds. HY25 estimated the significance of several individual regions to be between 2 and 4σ each, based on a comparison of bootstrapping samples from the entire dataset and background-only datasets. Several other emission hotspots in this band appear when the bright Milky Way foreground is masked out. At least six regions appear to lie far from the Milky Way plane. At least two of them may be associated with the Magellanic Stream and HVCs, as indicated in Fig. 2. The others are coincident with nearby galaxy groups in the regions around Andromeda, Ursa Major, Hydra/Sextans, and the Virgo Cluster.

We extracted the 511 keV fluxes from these six regions and combinations thereof by visually setting elliptical boundaries around the hotspots. While this method might be slightly biased, we used the bootstrapping samples to estimate confidence intervals for each selected region. In Sect. 4 we take only the galaxies into account that fall exactly into these ellipses, so that any in- or decrease of the regions is properly taken into account. The details about the regions we selected are found in Table 1.

The regions are indicated in Fig. 3, in which the HY25 map is shown again, together with all LVGs up to 30 Mpc. Most of these emission regions fall into low-exposure observations or are neighbouring high-exposure regions, so that a strong exposure gradient within only a few degrees across the sky emerges. While this is naturally handled by proper application of the imaging response function (IRF) in the RL reconstruction algorithm, it might still be the case that the IRF itself is flawed, that the instrumental background modelling approach (Diehl et al. 2018; Siegert et al. 2019b) still produces some systematics, or both. HY25 tested this masking of parts of the IRF that might be affected the strongest, that is, at large zenith angles beyond the field of view of 16°, and found that the resulting image was almost identical. While this is not direct proof that the response is correct, it shows that at large zenith angles, the far wings of the field of view have no significant impact on the resulting image. The background model relies on the fact that the geometry of the instrument does not change with time, so that the background pattern in the energy bin we studied only changed whenever a detector failed (for more details on background handling, we refer to HY25).

Because the exposure is non-uniform, the sensitivity varies across the map, and not every region can be treated equally. For this reason, HY25 performed a bootstrap sampling by generating many reconstructed images and adding Poisson fluctuations to the dataset. They also estimated the uncertainties for a flux from a certain region of interest. This also allowed us to estimate some sort of systematics or signal-to-noise ratio (significance) by taking into account background-only samples. We note that methods such as likelihood fitting can, in principle, account for correlations between pixels and the background. If the bootstrap samples were truly independent, this would similarly be ensured. However, because our approach adds noise to the real data, the degree to which sample independence is guaranteed is not straightforward. As a reference, comparing the bootstrap uncertainties with those from a model fitting approach for the total Galaxy flux, we found a difference of a factor of 2–3. Siegert et al. (2016a, 2019a), and Siegert et al. (2022) also showed that neglecting covariance terms can lead to an overestimation of the uncertainties by a factor of 2 or more. Given these considerations, the bootstrap uncertainties can in this case provide a conservative estimate. However, since we focused on the scientific interpretation and impact in the case of future confirmation and not on a detailed discussion of the detection significance, we used the bootstrap uncertainties throughout.

Based on the regions in Table 1, we estimated the 511 keV fluxes from the HY25 map and their uncertainties in Table 2. We show the resulting bootstrap distributions from resampling the dataset and the background-only in Fig. 5 for the combined regions of HVCs and LVGs. Clearly, the more nearby regions of the HVCs can hardly be explained by background fluctuations. The extragalactic sources have (even combined) a relatively small exposure so that there is no strong evidence that they are not be background fluctuations. However, several hotspots appear preferentially in directions towards large galaxy accumulations and nearby gas clouds. While this in itself is not statistically conclusive, this spatial coincidence motivates a physical interpretation, as discussed in the following (see Fig. 4 for a detailed view towards the Galactic poles).

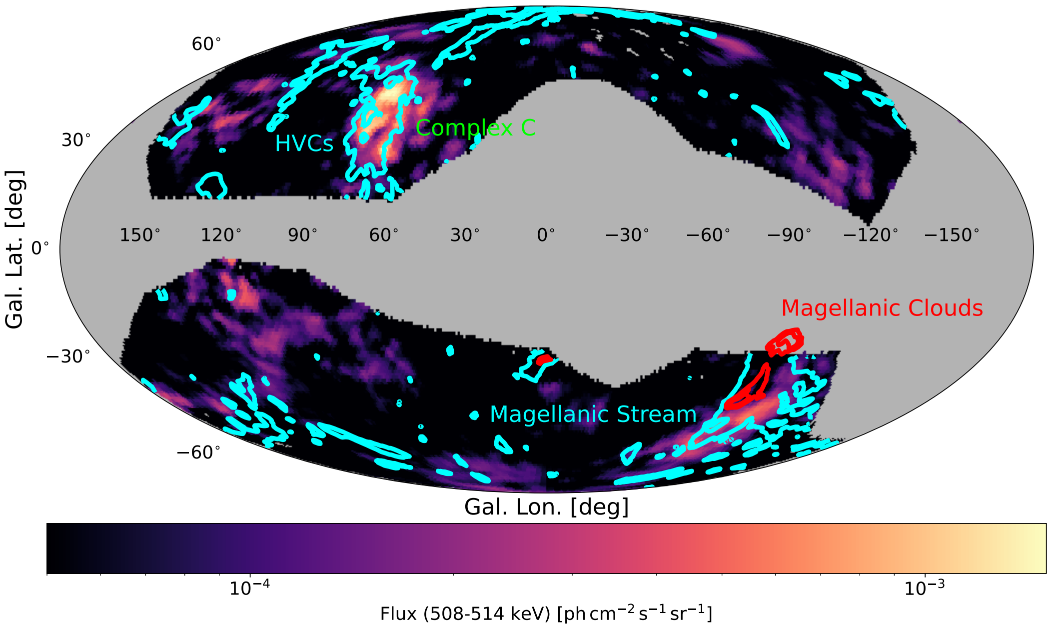

Fig. 2. RL 511 keV map from HY25 with the bright bulge and disk regions masked out (grey) to emphasise the low surface brightness region at high latitudes. The cyan contours show the HVCs of Westmeier (2018) at a hydrogen column density of 10^{19} cm^{-2}. The highest column densities around the Magellanic Clouds ($(\ell, b)_{\rm LMC} = (280.5^\circ, -32.9^\circ)$, $(\ell, b)_{\rm SMC} = (302.8^\circ, -44.3^\circ)$) are indicated in red at a level of 10^{20} cm^{-2}. The two strongest high-latitude 511 keV regions around $(\ell_0, b_0) \sim (70^\circ, 40^\circ)$ and $(\ell_0, b_0) \sim (-100^\circ, -55^\circ)$ largely coincide with the HVC Complex C and high-density parts of the Magellanic Stream, respectively. The other 511 keV emission regions may be associated with LVGs (see Fig. 3).

Table 1. Extragalactic regions with enhanced 511 keV flux.

Name	ℓ_0	b_0	a_0	e_0	θ_0	$d_0^\pm$	$d_1^\pm$	$d_2^\pm$	Comments
Complex C	70	40	17.5	0.515	0	0.004–0.012	–	–	HVC
Mag. Stream	−100	−55	25.0	0.866	−10	0.020–0.100	–	–	–
Andromeda	121	−21	23.0	0.000	0	0.020–0.040	0.52–1.31	2.5–12.5	nearby dSphs, M31 group, NGC 628/784 extended groups
Ursa Major	140	40	18.0	0.000	0	0.020–0.100	1.37–5.55	7.2–14.9	nearby dSphs, M81 group, NGC 2787/3556 ext. groups
Hydra	−115	30	20.0	0.662	25	0.080–0.150	1.29–1.45	8.2–23.0	nearby dSphs, NGC 3109 group, NGC 3115/2784 ext. groups
Virgo	−125	70	15.0	0.745	0	0.040–0.500	–	1.7–25.2	nearby dSphs, galaxies along line of sight, Virgo Cluster

Notes. The columns, from left to right, include the central Galactic longitude, ℓ_0, of an ellipse-shaped region in units of degrees, its Galactic latitude, b_0, in degrees, its semi-major axis, a_0, in degrees, its eccentricity, e_0, its position angle, θ_0, in degrees, three distance range estimates, $d_{0,1,2}^\pm$, of known features or sub-groups along the line of sight, in units of Mpc, and comments about associations. The table is split into possible annihilation in gas surrounding the Milky Way (top) and other galaxy groups (bottom).

3. Magellanic Stream and high-velocity clouds

Westmeier (2018) used the HI4PI dataset to extract the column densities and velocity profiles for Milky-Way-associated HVCs. We found that the two major regions in the HVC catalogue, the Magellanic Stream in the southern sky and Complex C in the northern sky, align well with the strongest 511 keV emission hotspots at higher latitudes, $|b| \gtrsim 15^\circ$. Based on the visual inspection in Sect. 2, we found 511 keV fluxes of $F_{\rm CC} = (9.1 \pm 2.6) \times 10^{-5}$ ph cm^{-2} s^{-1} for Complex C and $F_{\rm MS} = (4.9 \pm 1.6) \times 10^{-5}$ ph cm^{-2} s^{-1} for the Magellanic Stream region. The uncertainties were estimated from the bootstrapping samples. The combined flux of the two regions is $(14.0 \pm 3.1) \times 10^{-5}$ ph cm^{-2} s^{-1}. From the background-only bootstrap samples (Fig. 5, left), we estimated the expected background fluctuation to obtain a systematic uncertainty of 4.2×10^{-5} ph cm^{-2} s^{-1}. From the magnitude of these systematics, it appears unlikely that the two emission regions combined stem from background fluctuations. Based on the suggested distances of Complex C of 4–12 kpc (Wakker et al. 2007) and to the Magellanic Stream of 20–100 kpc (Mishra et al. 2025), the annihilation rates in the two regions are $(0.1{-}4.5) \times 10^{42}$ s^{-1} and $(0.8{-}156.3) \times 10^{42}$ s^{-1}, respectively. This assumes a minimum and maximum distance as well as annihilation through only Ps or only direct. If the annihilation conditions inside the clouds are similar to those in the interstellar medium (ISM), the values would be 1 and 34×10^{42} s^{-1}, respectively. The Magellanic Clouds themselves might contribute to the latter value with some unknown fraction. If the annihilation in the Magellanic Stream is solely fed by the Milky Way, the total Galactic annihilation rate would be at least the canonical value of 5×10^{43} s^{-1} (Siegert et al. 2016a) plus the halo / HVC contributions. We explain this below. Considering that these regions only cover about 6% of the high latitude regions of the sky, a Galactic outflow of positrons might be about $(5{-}7) \times 10^{44}$ s^{-1}, that is, potentially stronger by more than ten times than the Galactic value. We assumed isotropic leakage from the Milky Way, which might in reality be affected by the intergalactic magnetic field. If the annihilation in the Magellanic Stream is fed by processes in the Large and Small Magellanic Clouds as major, that is, most nearby and brightest, contributors

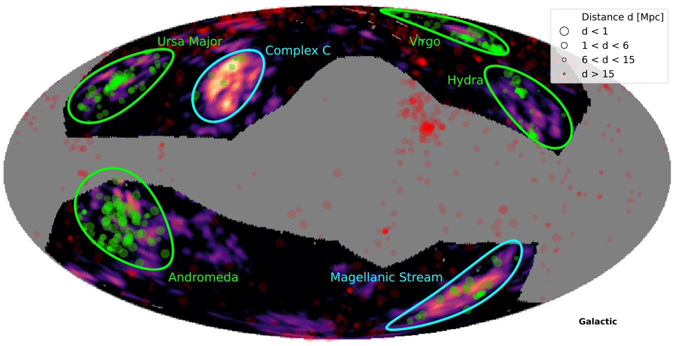

Fig. 3. Selected regions (ellipses) on top of the masked HY25 511 keV map. We show the distribution of all known (∼1600) LVGs up to a distance of 30 Mpc in red outside and in green inside the LVG regions (green). The distance intervals are indicated as marker sizes.

Table 2. Measured 511 keV fluxes in the regions of interest.

Name	F_{511}	$p2.5$	$p16$	$p50$	$p86$	$p97.5$
Complex C	9.1	3.6	5.2	7.2	10.3	14.0
Mag. Stream	4.9	2.0	3.0	4.4	6.4	9.0
Combined	14.0	7.2	9.3	12.1	15.5	19.9
Andromeda	4.3	3.0	3.9	5.2	7.1	9.5
Ursa Major	2.4	1.2	1.8	2.8	4.4	6.9
Hydra	2.5	1.4	2.0	2.7	3.7	5.4
Virgo	0.8	0.4	0.6	0.9	1.5	2.5
Combined	10.1	8.6	10.1	12.3	14.9	17.8
All combined	24.0	18.2	20.9	24.8	28.5	33.5

Notes. The columns include the integrated fluxes from the HY25 map in the energy bin 508–514 keV in units of 10^{-5} ph cm^{-2} s^{-1} and the confidence intervals (with $p2.5$ being the 2.5% percentile, etc.) from the bootstrapping samples in the same units.

in this region and not by the Milky Way alone, the Galactic outflow of positrons would carry about $(3–4) \times 10^{43}$ s^{-1}. The latter configuration agrees better with a leaky-box model of the sub-GeV cosmic-ray content of galaxies with escape fractions of 0.1−0.4 (Lacki et al. 2010; Yoast-Hull et al. 2013), which would be closer to our value of 0.4−0.5 when only Complex C were included, rather than ≳90% for the two regions combined. However, Webber (2015) estimated that based on the Voyager cosmic-ray electron spectrum, electrons with energies ≲30 MeV might escape in much larger fractions (≳90%). For positrons, this fraction is probably much lower because of the annihilation on the way. A total Galactic positron production rate based on the measured annihilation rate inside the ISM and in HVCs of $\sim 10^{44}$ s^{-1} therefore seems possible. We use this as a canonical value for further discussion.

4. Cumulative nearby extragalactic signal

In addition to the two bright hotspots that may be aligned with HVCs and the Magellanic Stream, there are at least four low surface-bright 511 keV emission regions. We found that they align particularly well with nearby galaxy accumulations from the LVG catalogue (Karachentsev et al. 2004; Karachentsev 2005; Karachentsev et al. 2013) of almost 1600 galaxies up to 30 Mpc. We name the four regions for their major constellation, Andromeda, Ursa Major, Hydra, and Virgo. The measured 511 keV fluxes in the regions are typically very uncertain, with $(4.3 \pm 1.6) \times 10^{-5}$ ph cm^{-2} s^{-1}, $(2.4 \pm 1.3) \times 10^{-5}$ ph cm^{-2} s^{-1}, $(2.5 \pm 0.9) \times 10^{-5}$ ph cm^{-2} s^{-1}, and $(0.8 \pm 0.5) \times 10^{-5}$ ph cm^{-2} s^{-1}, respectively. The right panel of Fig. 5 shows that the combined flux of these four regions itself is rather significant at $(10.1 \pm 2.4) \times 10^{-5}$ ph cm^{-2} s^{-1}, but that the systematic uncertainty estimated from the background-only samples is also of the order of the flux itself. There is a high probability that even these four regions combined are due to background fluctuations. However, as noted above, the exposure of 20 years of INTEGRAL/SPI observations is quite anisotropic, so that, on one hand, only flux can be detected when the region was actually observed, but on the other hand, the large gradients in the exposure may lead to several artefacts. We continue the discussion based on the extracted RL values.

Because the extended extragalactic emission regions might originate from the cumulative effect of many sources at different distances along the line of sight, there is no single annihilation rate per source region. Instead, the properties of the typically ∼100 LVGs in each region can be used to perform a Bayesian hierarchical decomposition of the measured fluxes into per-source fluxes. By assuming a simple power-law scaling of the B-band luminosity, $L_{B,i}$, of the sources, and taking into account their distances, d_i, we performed a decomposition by estimating the total source region flux as the sum of the individual LVGs, $F_{i,r}$, as

$$F_{\mathrm{est},r} = \sum_{i=1}^{N_r} F_{\mathrm{est},i,r} = \sum_{i=1}^{N_r} R_{\mathrm{MW}} \frac{(L_{B,i}/L_{B,\mathrm{MW}})^{\gamma}}{4\pi d_i^2}. \quad (1)$$

We normalised by our estimated annihilation rate in the Milky Way, $R_{\mathrm{MW}} \sim 10^{44}$ e$^+$ s^{-1}, and its B-band luminosity, $L_{B,\mathrm{MW}} = 2.5 \times 10^{10}\,L_{B,\odot}$, and we fitted for the index γ to obtain a per-source-flux and therefore annihilation rate. We assumed that the observed fluxes, $F_{\mathrm{obs,r}}$, per region r follow a log-normal distribution, $\ln F_{\mathrm{obs,r}} \sim \mathcal{N}\left(\ln F_{\mathrm{obs},r}, \sigma_r^2\right)$, where the total uncertainty per region is $\sigma_r = \sigma_{F,r}/F_{\mathrm{obs},r}$. Each source was assigned some intrinsic scatter, σ_{src}, so that $\ln F_{i,r} \sim \mathcal{N}(\ln F_{\mathrm{est},i,r}, \sigma^2_{\mathrm{src}})$. We chose $\sigma_{\mathrm{src}} \sim$ HalfNormal(0.5), which means allowing half an order of magnitude in both directions for the intrinsic scatter of each individual source. Finally, we set a prior on $\gamma \sim \mathcal{N}(1, 1)$ for our parameter of interest.

We found a scaling relation like $L_{511} \propto L_B^{\gamma}$ with $\gamma = 0.25 \pm 0.03$. With this scaling, the total predicted fluxes of the four regions are 2.4 ± 1.0 for 98 LVG sources, 2.0 ± 0.9 for 100, 1.1 ± 0.6 for 67, and $(1.1 \pm 0.3) \times 10^{-5}$ ph cm^{-2} s^{-1} for 154 sources, respectively. This is somewhat on the low side of the individual regions, indicating potentially missing sources, hidden variables in addition to a scaling with L_B, or different annihilation conditions that might lead to larger or smaller line components from positron annihilation. For each galaxy in our selection, we show the expected 511 keV flux in Fig. 6. All annihilation rates would range between 10^{41} and 10^{45} s^{-1} for any type of galaxy using this scaling relation. About ten sources might have a higher flux than 10^{-6} ph cm^{-2} s^{-1}, including M31, M33, IC 10, and NGC 0185 in the Andromeda region, and four sources more than 10^{-5} ph cm^{-2} s^{-1}, all of them being dwarf galaxies with Triangulum II and Ursa Major II showing the highest fluxes around 2×10^{-5} ph cm^{-2} s^{-1}. When we compare these values with the 511 keV study from Siegert et al. (2016b), all values are still consistent, that is below, with previous upper limits. Clearly, with a more uniform exposure and/or higher sensitivity, these sources may be readily seen with the next generation MeV telescopes, and in particular, with COSI (Tomsick et al. 2024).

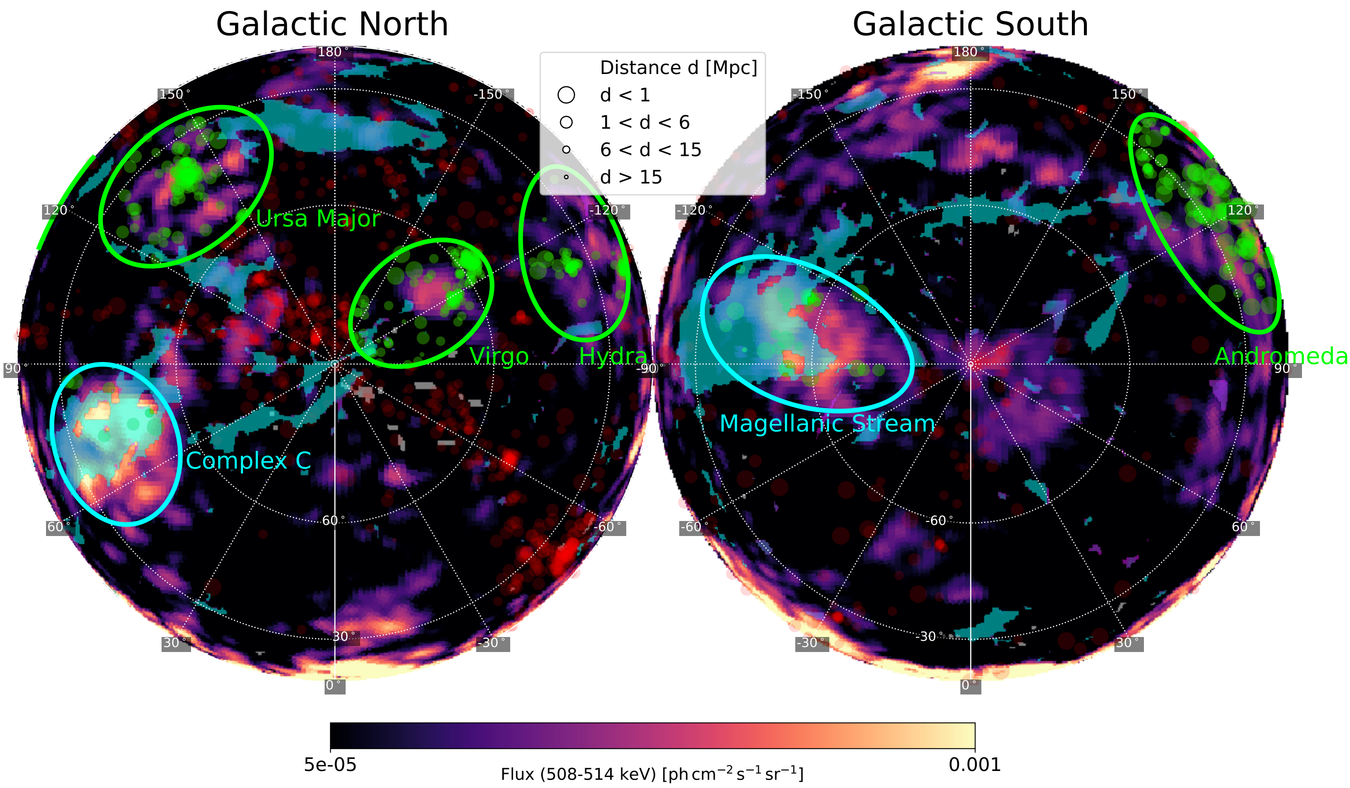

Fig. 4. Same as Figs. 2 and 3, now combined in orthographic projection to emphasise the Galactic poles. The Galactic North is shown on the left, and the Galactic South is shown on the right. All regions are marked as before, with the Magellanic Stream as a cyan overlay. The Galactic centre and bulge are visible as the bright region at the bottom of both panels.

5. Cosmological positron annihilation signal

If future 511 keV observations, such as those planned with the Compton Spectrometer and Imager (COSI Tomsick et al. 2024), were to confirm the tantalising hints discussed above, such as the total positron production rate in the Milky Way and the 511 keV emission from LVGs, we would be able to further discuss some first-order expectations of positron annihilation to the CGB. Beyond 25–200 Mpc, the cumulative nearby extragalactic signal is expected to morph into a quasi-isotropic cosmological positron annihilation spectrum. Then, the redshift z needs to be taken into account and a cosmological model assumed for the positron annihilation background calculation. By assuming $L_{511} \propto L_B^{\gamma} \propto \mathrm{SFR}^{\gamma}$, we can integrate the expected positron annihilation signal in the Universe from galaxies. While this might not be the only contribution to cosmological positron annihilation as other source classes and intergalactic medium effects might occur, this calculation serves as a first order-of-magnitude estimate of positron annihilation to the CGB.

The total quasi-isotropic positron annihilation flux from galaxies assuming a relation to their SFR is calculated by

$$\frac{dI(E_{\mathrm{obs}})}{dE_{\mathrm{obs}}} = \frac{c}{4\pi}\int_0^{z_{\max}} \frac{\dot{n}(z, R_{\mathrm{MW}}, \mathrm{SFR}_{\mathrm{MW}}, \gamma)\cdot S_{\mathrm{em}}\left(E_{\mathrm{em}}, f_{\mathrm{Ps}}, E_{\mathrm{inj}}\right)}{H(z)\cdot(1+z)}dz. \quad (2)$$

In Eq. (2), $\dot{n}(z, R_{\mathrm{MW}}, \mathrm{SFR}_{\mathrm{MW}}, \gamma)$ is the positron annihilation rate in galaxies as a function of redshift, and defined by scalings of the Milky Way annihilation rate R_{MW} and its SFR $\mathrm{SFR}_{\mathrm{MW}}$. We used

$$\dot{n}(z, R_{\mathrm{MW}}, \mathrm{SFR}_{\mathrm{MW}}, \gamma) = \frac{R_{\mathrm{MW}}}{\mathrm{SFR}_{\mathrm{MW}}}\cdot\rho_{\mathrm{SFR}}(z=0)\left(\frac{\rho_{\mathrm{SFR}}(z)}{\rho_{\mathrm{SFR}}(z=0)}\right)^{\gamma}, \quad (3)$$

where

$$\rho_{\mathrm{SFR}}(z) = 0.015\frac{(1+z)^{2.7}}{1+\left(\frac{1+z}{2.9}\right)^{5.6}}\,\mathrm{M}_{\odot}\,\mathrm{yr}^{-1}\,\mathrm{Mpc}^{-3} \quad (4)$$

is the SFR history of the Universe from Madau & Dickinson (2014). While γ is suggested to be close to 0.25 from Sect. 4, the true dependence is unknown, and we calculated the expected cumulative signal for a range of γ values. There might also be hidden variables such as the total mass of galaxies, their dark matter content, a delay-time distribution to take account the old stellar population, et cetera, but this might largely over-interpret the current findings. For this reason, we kept this calculation as simple as possible and refer to future works for more detailed models. We used a standard cosmological model with a Hubble parameter defined as

$$H(z) = H_0\sqrt{\Omega_m(1+z)^3+\Omega_\Lambda}, \quad (5)$$

with $\Omega_m = 1 - \Omega_\Lambda = 0.315$ and a Hubble constant of $H_0 = 67.4\,\mathrm{km\,s^{-1}\,Mpc^{-1}}$.

We assumed a positron annihilation spectrum similar to that of the Milky Way with a 511 keV line, an ortho-Ps continuum, and annihilation in flight. For this, we defined the following functions: The survival probability of not annihilating in flight is given by

$$P_{\mathrm{surv}} = P_{\mathrm{surv}}\left(E_{\mathrm{inj}} \to \eta\cdot m_e\right) = \exp\left[-n_X J(E_{\mathrm{inj}})\right], \quad (6)$$

with

$$J(E) = \int_{\eta\cdot m_e}^{E}\frac{\sigma(E')}{(dE'/dx)}\,dE' \quad (7)$$

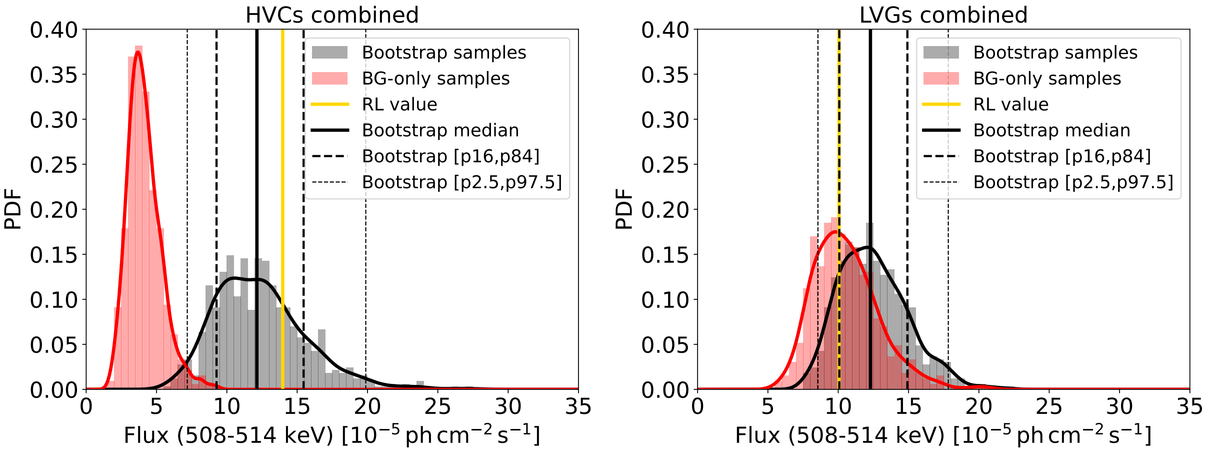

Fig. 5. Bootstrapping samples for the combined regions of HVCs (Complex C and Magellanic Stream; left) and selected LVGs (Andromeda, Ursa Major, Hydra, and Virgo; right). We show the samples for the entire dataset (grey histogram) and background-only (red), together with the 68.3 (dashed) and 95.4% (dotted) confidence intervals and the true RL value (gold vertical line).

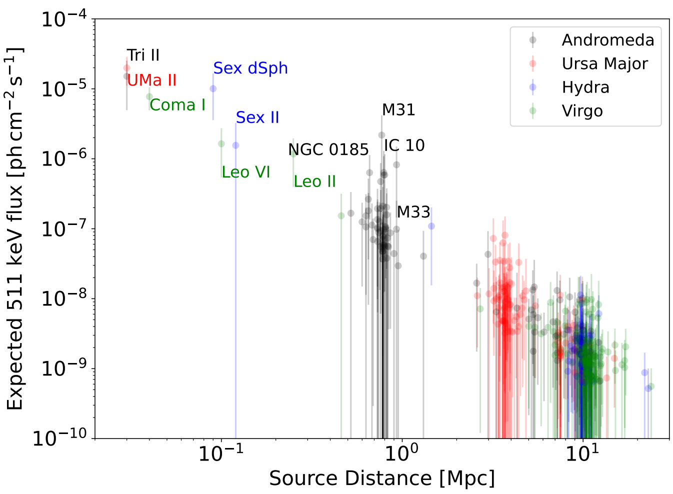

Fig. 6. Expected 511 keV fluxes from individual sources within the bright regions. The fluxes originate from a Bayesian hierarchical decomposition assuming a relation with a galaxy's blue-band luminosity, Eq. (1). Sources with an expected flux stronger than 10^{-6} ph cm^{-2} s^{-1} are named.

being the path integral of the total annihilation cross section along the slowing-down trajectory per unit target density. In other words, the exponent in Eq. (6) is an optical depth along the track of positrons. The factor η was set to account for the thermalisation threshold for positrons in the ISM, typically below 1 keV, so that we set $\eta = 1.001$ in all following calculations. We note that the choice of η does not change the results unless it is set to values much higher than 1.001.

The number of photons per unit annihilation event was calculated as

$$r_{\rm Line} = P_{\rm surv}\left(2 - \frac{3}{2} f_{\rm Ps}\right) \tag{8}$$

for the 511 keV line,

$$r_{\rm oPs} = P_{\rm surv}\left(\frac{9}{4} f_{\rm Ps}\right) \tag{9}$$

for the ortho-Ps continuum, and

$$r_{\rm IA} = 2\,(1 - P_{\rm surv}) \tag{10}$$

for the in-flight annihilation component. In typical ISM conditions where ionisation losses on hydrogen dominate and for positron injection energies in the MeV range, $P_{\rm surv}$ is between 81% ($E_{\rm inj} = 50$ MeV) and 96% ($E_{\rm inj} = 2$ MeV). The Ps fraction, $f_{\rm Ps}$, carries the details about the ISM conditions and is typically found to be close to the maximum of 1.0 in the Milky Way. We set it to a generic value of $f_{\rm Ps} = 0.92$ given annihilation spectroscopy studies within the last 50 years (see Siegert 2023, for a recent review).

For natural units ($c = 1$) and with a positron mass of $m_e = 511$ keV, the generic spectral shapes for the annihilation line are

$$L(E_{\rm em}) = \frac{1}{\sqrt{2\pi}\sigma} \exp\left(-\frac{1}{2}\left[\frac{E_{\rm em} - m_e}{\sigma}\right]^2\right), \tag{11}$$

for the ortho-Ps component (Ore & Powell 1949)

$$O(E_{\rm em}) = \frac{2}{m_e\,(\pi^2 - 9)}\left[\frac{E_{\rm em}(m_e - E_{\rm em})}{(2m_e - E_{\rm em})^2} + \frac{2m_e - E_{\rm em}}{E_{\rm em}} + \left(\frac{2m_e(m_e - E_{\rm em})}{E_{\rm em}^2} - \frac{2m_e(m_e - E_{\rm em})^2}{(2m_e - E_{\rm em})^3}\right)\right], \tag{12}$$

and for the in-flight annihilation spectrum

$$A(E_{\rm em}) = \frac{n_e}{1 - P_{\rm surv}(E_{\rm inj}, \eta \cdot m_e)} \times \int_{E_1(E_{\rm em})}^{E_{\rm inj}} \frac{P_{\rm surv}(E_{\rm inj}, E_+)}{m_e} \frac{\frac{d\sigma}{dk}(\gamma(E_+), k(E_{\rm em}))}{\left(\frac{dE_+}{dx}\right)(E_+, n_X)} \, dE_+, \tag{13}$$

where we caution that, in general, the electron density, n_e, and the density in which the positrons slow down, n_X with $X =$ H, He, Na, ... (Panther et al. 2018), are not necessarily the same. The reason for using $n_e = n_X$ here, and which was also true in previous studies (e.g., Churazov et al. 2005; Beacom & Yüksel 2006; Sizun et al. 2006; Knödlseder et al. 2025), is that the dependence on the densities cancels in Eq. (13), which makes it more analytically tractable. For higher positron energies or much lower densities, such as in the intergalactic medium, mostly

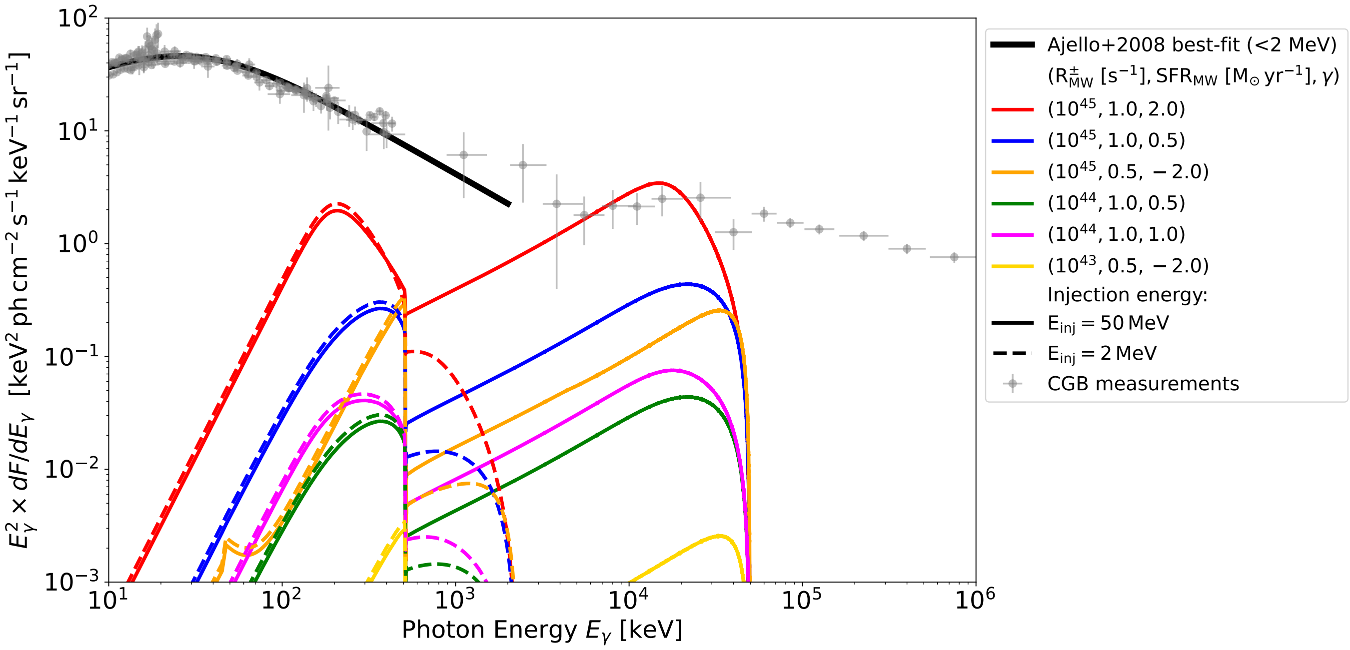

Fig. 7. Cosmological positron annihilation signal assuming Eq. (2) for different assumptions on the total Galactic positron production (= pair annihilation) rate, $R^{\pm}_{MW}$, different Galactic SFRs, SFR$_{MW}$, and dependences on the SFR history, γ. Two different but generic positron injection energies are shown. The Ps fraction is set to $f_{Ps} = 0.92$ in both cases. We note that this is not the only contribution to the cosmological positron annihilation spectrum and only assumes some link to SFR. Isotropic Galactic contributions are ignored.

inverse-Compton and synchrotron losses would shape the in-flight annihilation spectrum, rather than ionisation losses and Coulomb scattering in plasmas. The differential cross section $\frac{d\sigma}{dk}(\gamma(E_+), k(E_{em}))$ as well as the integration limits and variable definitions are the same as in Beacom & Yüksel (2006).

The spectral functions were normalised to 1.0,

$$\int L(E)\,dE = \int O(E)\,dE = \int A(E)\,dE = 1. \quad (14)$$

The total emission spectrum was then

$$S_{em}\left(E_{em}, f_{Ps}, E_{inj}\right) = r_{Line}L(E_{em}) + r_{oPs}O(E_{em}) + r_{IA}A(E_{em}), \quad (15)$$

so that integrating over the photon energy gave

$$\int S_{em}(E_{em})\,dE = r_{Line} + r_{oPs} + r_{IA} \equiv N_\gamma, \quad (16)$$

which is simply the average number of photons emitted per electron-positron annihilation event. This led to spectra as shown in Fig. 7.

Because of the true dependence on the SFR, and also that of other parameters, is unknown, we might constrain them by measuring the CGB to a much higher accuracy than currently achieved. We note that there would also be an isotropic 511 keV line as well as the other annihilation components from the Milky Way itself because the observer sits inside. This would add to cosmological isotropic component, but is also beyond the scope of this work.

If the total positron annihilation rate of the Milky Way is about 10^{44} s^{-1} or above, which might be suggested by this work, some imprint on the CGB might be expected already from this component. With the future launch of COSI in 2027, the CGB can be measured with a much higher accuracy in the MeV range, so that any indications of a sharp cut-off at 511 keV, a rising spectrum below 511 keV, or a rising spectrum in the 1–5 MeV range can indicate a cosmological positron annihilation component. Clearly, other long-sought CGB components, such as the cumulative cosmological spectrum of type Ia supernovae (e.g., Ruiz-Lapuente et al. 2016), kilonovae (e.g., Ruiz-Lapuente & Korobkin 2020), IGM processes (Gelowicz et al., in prep.), and the Milky Way (Siegert 2023) and Local Bubble (Siegert et al. 2024) foreground will add, so that only with detailed modelling and a proper statistical data analysis, the different components will be deciphered.

6. Summary and conclusions

We analysed the high-latitude regions of the HY25 511 keV map and found six emission hotspots with a combined flux of $(24.0 \pm 3.8_{stat} \pm 14.3_{syst}) \times 10^{-5}$ ph cm^{-2} s^{-1}. We separated this flux into regions coincident with HVCs and the Magellanic Stream showing a flux of $(14.0 \pm 3.1_{stat} \pm 4.2_{syst}) \times 10^{-5}$ ph cm^{-2} s^{-1}, and coincident with LVGs with a flux of $(10.1 \pm 2.4_{stat} \pm 10.1_{syst}) \times 10^{-5}$ ph cm^{-2} s^{-1}. The statistical and systematic uncertainties are estimated from bootstrap sampling of the entire dataset and background-only realisations. Based on these numbers and the coincident regions, we suggest that the Milky Way might show significant outflows of material carrying positrons, which would enhance the total positron production rate up to 10^{44} s^{-1}, which is about a factor of 2–3 higher than from measurements inside the interstellar medium. A possible cumulative extragalactic positron annihilation signal from nearby galaxy groups, such as around Andromeda, Ursa Major, Hydra/Sextans, and Virgo might explain the remaining signal. We perform a Bayesian flux decomposition of the emission regions using all known LVGs up to a distance of 30 Mpc and find consistency if the galaxies' 511 keV flux scales with their B-band luminosity as $\propto L_B^{0.25\pm0.03}$. Then, all galaxies would show intrinsic annihilation rates between 10^{41} and 10^{45} s^{-1}. Based on this decomposition, several sources with 511 keV fluxes above 10^{-6} ph cm^{-2} s^{-1}, including Triangulum II, Ursa Major II, Sextans dwarf spheroidal, M31, and M33, among others, might be identified as individual sources with next generation telescopes, such as COSI (Tomsick et al. 2024). Taking this model one step ahead, we calculate the cosmological contribution of positron annihilation in galaxies, assuming some dependency on the SFR. We estimate that this contribution is probably sub-dominant on the per-cent level, however might show some imprints on the ten per-cent level if the intrinsic positron injection energy is tens of MeV or higher. We note that this is probably not the only cosmological or isotropic positron annihilation component, and we will address this in forthcoming works (Gelowicz et al., in prep.). While there is still a chance that some high-latitude 511 keV emission features are imaging artefacts, it appears at odds if all hotspots are mere background fluctuations.

References

Beacom, J. F., & Yüksel, H. 2006, Phys. Rev. Lett., 97, 071102
Churazov, E., Sunyaev, R., Sazonov, S., Revnivtsev, M., & Varshalovich, D. 2005, MNRAS, 357, 1377
Diehl, R., Siegert, T., Greiner, J., et al. 2018, A&A, 611, A12
Karachentsev, I. D. 2005, AJ, 129, 178
Karachentsev, I. D., Karachentseva, V. E., Huchtmeier, W. K., & Makarov, D. I. 2004, AJ, 127, 2031
Karachentsev, I. D., Makarov, D. I., & Kaisina, E. I. 2013, AJ, 145, 101
Kierans, C. A., Boggs, S. E., Chiu, J. L., et al. 2017, arXiv e-prints [arXiv:1701.05558]
Knödlseder, J., Sabri, K., Jean, P., et al. 2025, A&A, 700, A257
Lacki, B. C., Thompson, T. A., & Quataert, E. 2010, ApJ, 717, 1
Madau, P., & Dickinson, M. 2014, ARA&A, 52, 415
Mishra, S., Fox, A. J., Smoker, J. V., Lucchini, S., & D'Onghia, E. 2025, ApJ, 984, 104
Ore, A., & Powell, J. L. 1949, Phys. Rev., 75, 1696
Panther, F. H., Seitenzahl, I. R., Crocker, R. M., et al. 2018, Phys. Rev. D, 98, 023015
Ruiz-Lapuente, P., & Korobkin, O. 2020, ApJ, 892, 45
Ruiz-Lapuente, P., The, L.-S., Hartmann, D. H., et al. 2016, ApJ, 820, 142
Siegert, T. 2023, Ap&SS, 368, 27
Siegert, T., Diehl, R., Khachatryan, G., et al. 2016a, A&A, 586, A84
Siegert, T., Diehl, R., Vincent, A. C., et al. 2016b, A&A, 595, A25
Siegert, T., Crocker, R. M., Diehl, R., et al. 2019a, A&A, 627, A126
Siegert, T., Diehl, R., Weinberger, C., et al. 2019b, A&A, 626, A73
Siegert, T., Boggs, S. E., Tomsick, J. A., et al. 2020, ApJ, 897, 45
Siegert, T., Crocker, R. M., Macias, O., et al. 2022, MNRAS, 509, L11
Siegert, T., Schulreich, M. M., Bauer, N., et al. 2024, A&A, 689, A2
Sizun, P., Cassé, M., & Schanne, S. 2006, Phys. Rev. D, 74, 063514
Tomsick, J., Boggs, S., Zoglauer, A., et al. 2024, in 38th International Cosmic Ray Conference, 745
Vedrenne, G., Roques, J.-P., Schönfelder, V., et al. 2003, A&A, 411, L63
Wakker, B. P., York, D. G., Howk, J. C., et al. 2007, ApJ, 670, L113
Webber, W. R. 2015, arXiv e-prints [arXiv:1508.06237]
Westmeier, T. 2018, MNRAS, 474, 289
Winkler, C., Courvoisier, T. J.-L., Di Cocco, G., et al. 2003, A&A, 411, L1
Yoast-Hull, T. M., Everett, J. E., Gallagher, J. S., III, & Zweibel, E. G. 2013, ApJ, 768, 53
Yoneda, H., Siegert, T., & Mittal, S. 2025, A&A, 702, A220